PERGAMON

Journal of Structural Geology 22 (2000) 1649–1661

JOURNAL OF STRUCTURAL GEOLOGY

www.elsevier.nl/locate/jstrugeo

Crystallographic preferred orientation in albite samples deformed experimentally by dislocation and solution precipitation creep

Florian Heidelbach[a,*], Alice Post[b], Jan Tullis[c]

[a]*Bayerisches Geoinstitut, Universität Bayreuth, D-95440, Bayreuth, Germany*
[b]*Institut für Geologie – Endogene Dynamik, RWTH Aachen, D-52056, Aachen, Germany*
[c]*Department of Geological Sciences, Brown University, Providence, RI 02912, USA*

Received 30 November 1999; accepted 24 May 2000

Abstract

The crystallographic preferred orientations of a series of experimentally deformed fine-grained albite aggregates were measured by synchrotron source X-ray diffraction. Most samples were deformed and extensively recrystallized by low-temperature recrystallization-accommodated dislocation creep. In axial compression as well as simple shear these samples developed weak but distinct crystallographic preferred orientations consistent with intracrystalline slip on $\{001\} < 100 >$; the sheared samples have a marked asymmetry of the $<100>$ maxima with respect to the shear zone boundaries. One sample was axially compressed by solution precipitation creep; it developed a somewhat different but equally strong preferred orientation, perhaps reflecting crystallographic anisotropy in rates of dissolution and growth.

1. Introduction

Crystallographic preferred orientations (CPOs or textures) are often used to infer aspects of the thermo-mechanical history of rocks, because the texture pattern that develops during deformation is a function of the deformation geometry as well as the deformation mechanism or creep regime. Experiments and modelling have been used to link CPO patterns to deformation conditions and geometry (e.g. Lister and Hobbs, 1980). CPOs measured in experimentally deformed samples have been combined with transmission electron microscopy (TEM) observations and mechanical data to determine the dominant slip systems and the role of dynamic recrystallization (e.g. Tullis et al., 1973, Schmid et al., 1987, Gleason et al., 1993).

Most of the work that has been done on CPOs of minerals has concentrated on those with a relatively simple crystallography, such as quartz and calcite. Several studies have linked CPO patterns to the operation of specific slip systems. In quartz, for example, basal slip is the dominant system at lower temperatures; in pure shear this slip system produces a *c*-axis maximum perpendicular to the flattening plane (e.g. Schmid, 1994 and references therein), whereas in simple shear it often produces a *c*-axis maximum asymmetrically inclined to the shear plane (e.g. Dell'Angelo and Tullis, 1989). For deformation at higher temperatures and slower strain rates there appears to be a transition to slip on the prism and rhombohedral planes, as inferred from small circle distributions of *c* axes around the compression axis (e.g. Tullis et al., 1973) and *c* maxima within the flattening or shear plane (e.g. Mainprice et al., 1986).

The effect of dynamic recrystallization on CPOs has been a topic of recent interest. In quartz aggregates, CPO patterns have been measured in the deformed and recrystallized grains of samples experimentally deformed in different dislocation creep regimes (Gleason et al., 1993). With increasing temperature, or decreasing strain rate, the recrystallization mechanism accompanying dislocation creep changes from slow grain boundary bulging through subgrain rotation to fast grain boundary migration (Hirth and Tullis, 1992). Gleason et al. (1993) showed that the CPO pattern of the recrystallized grains is different from that of deformed original grains in the low-temperature regime, indicating that dynamic recrystallization can change the pattern produced by slip alone. Other minerals, including feldspar, appear to show similarly distinct dislocation creep regimes, characterized by different mechanisms of dynamic recrystallization (Tullis, 1990), but there are no systematic studies investigating how these affect the CPOs developed.

Despite the abundance of plagioclase in the crust, including medium- to high-temperature mylonitic rocks, relatively little is known about the CPOs that develop during

* Corresponding author.

0191-8141/00/$ - see front matter
PII: S0191-8141(00)00072-9

deformation and recrystallization in these minerals. This lack of data is mainly due to two factors: (i) their chemical variability (from $NaAlSi_3O_8$ to $CaAl_2Si_2O_8$) which is accompanied by a continuous change in lattice parameters; and (ii) their triclinic symmetry. Due to these complications most studies of CPOs in naturally deformed plagioclase have used light microscope U-stage goniometry; under favorable circumstances this technique allows the determination of the complete crystal orientation, but it is very time consuming and impossible for small grain sizes (<25 μm).

In this study we present the first measurements of CPO patterns in experimentally deformed fine-grained albite aggregates. The patterns were measured using a high-intensity synchrotron X-ray beam, in combination with a two-dimensional charge-coupled device (CCD) detector. We report CPO patterns developed in axial shortening as well as in simple shear, and for samples that were deformed by solution-precipitation creep as well as by recrystallization-accommodated dislocation creep. These results are compared with patterns reported from naturally deformed samples.

2. Experimental

2.1. Starting material

The experiments were performed on polycrystalline aggregates of albitic feldspar ($Ab_{98}An_1Or_1$). Albite rock was obtained from the border zone of the Hale pegmatite in Connecticut. Some albite was crushed and the 2–10 μm size fraction separated by settling in distilled water. After separation the powder was washed in alcohol and dried in an oven at 100°C. Weight loss upon vacuum drying at 300°C and 6 Pa indicated that the powder contained approximately 0.1 wt.% adsorbed water. Most samples were prepared by hot-pressing in situ at 900°C and 1000–1500 MPa for 10 h prior to deformation; TEM shows that this 'starting material' has tight grain boundaries (indicating a porosity of <1%) and equidimensional grains with a high dislocation density ($\sim 10^{15}/m^2$, Fig. 1a). One experiment (RD33) was performed on a core of the Hale albite rock. This material has equant, randomly oriented grains averaging 150 μm in diameter with <1% impurities.

2.2. Deformation experiments

Most samples for axial compression experiments were prepared by loading the 2–10-μm Hale albite powder into a 6-mm diameter Pt 'can' and cold compacting it using a steel rod. For one experiment (W479) the powder was vacuum dried at 200°C for 6 h before mechanically sealing the top end of the Pt container, and for another (W484) the powder was vacuum dried at 300°C for 6 h and then weld-sealed in a Pt container; all other experiments utilized 'as-is' powder, with approximately 0.1 wt.% adsorbed water. For simple shear experiments, cores of Tanco albite rock cut at 30° to the long axis were used as the forcing blocks, and a layer of 'as-is' 2–10 μm albite powder from ~200 to ~400 μm thick was placed between the blocks. Axial compression of the pistons resulted in simple shear of the hot-pressed plagioclase aggregate. Details of this experimental set-up can be found in Post and Tullis (1999).

All but one (W484) of the samples were mechanically sealed in thin-walled Pt jackets, and outer sleeves of thin-walled Ni or Cu were used to align the sample with the pistons. All experiments were performed in a Griggs-type solid medium apparatus, using NaCl as the confining medium. The experiments were performed at 900°C, but the deformation geometry, strain rate, pressure and water content were varied in order to produce samples with different deformation histories. The deformation conditions and geometries are listed in Table 1.

In one experiment a shear zone of fine-grained albite was produced in a different way. A solid core of Hale albite rock (mechanically sealed in Pt with 0.1 wt.% water added) was loaded at 300°C, 500 MPa and 10^{-4}/s until it faulted at roughly 30° to compression; a short distance of sliding produced a small amount of fine-grained fault gouge. The load was then removed, and the sample was taken to 900°C and 1500 MPa, where the gouge was 'hot-pressed' into a tight aggregate. The sample was then deformed; all of the sample strain was partitioned into the thin fine-grained zone, resulting in an effective shear strain rate of $\sim 5 \times 10^{-4}$/s and producing an extremely localized ductile shear zone (see Tullis et al., 1990, for details).

2.3. Texture analysis

Textures in plagioclase have traditionally been measured with an optical microscope and a U-stage (e.g. Kruhl, 1987a,b; Ji et al., 1994). With this method the optical axes (α, β, γ) of single plagioclase grains can be measured; the orientation of the crystal lattice can then be uniquely reconstructed if the chemical composition and the orientation of one or more additional structural elements such as cleavage or twin planes are known (Burri et al., 1967). The method is therefore fairly time consuming and is restricted to relatively large grain sizes (>25 μm).

Recently electron backscattering techniques (EBSP) have been used successfully to measure the CPO of a plagioclase mylonite in the scanning electron microscope (SEM) (Prior and Wheeler, 1999). Neutron diffraction measurements of bulk samples have also successfully yielded CPO data for plagioclase, due to their high resolution in the diffraction angle 2Θ (Wenk et al., 1986; Wenk and Pannetier, 1990; Siegesmund et al., 1994; Ullemeyer et al., 1994). However, relatively large volumes of sample material (>1 cm^3) are needed for this type of measurement because neutron flux densities are low compared with X-ray sources.

In standard X-ray goniometry with a cathode tube source the beam size is about 1 mm^2, which is too large for our purposes; reducing the size of the beam leads to diminished

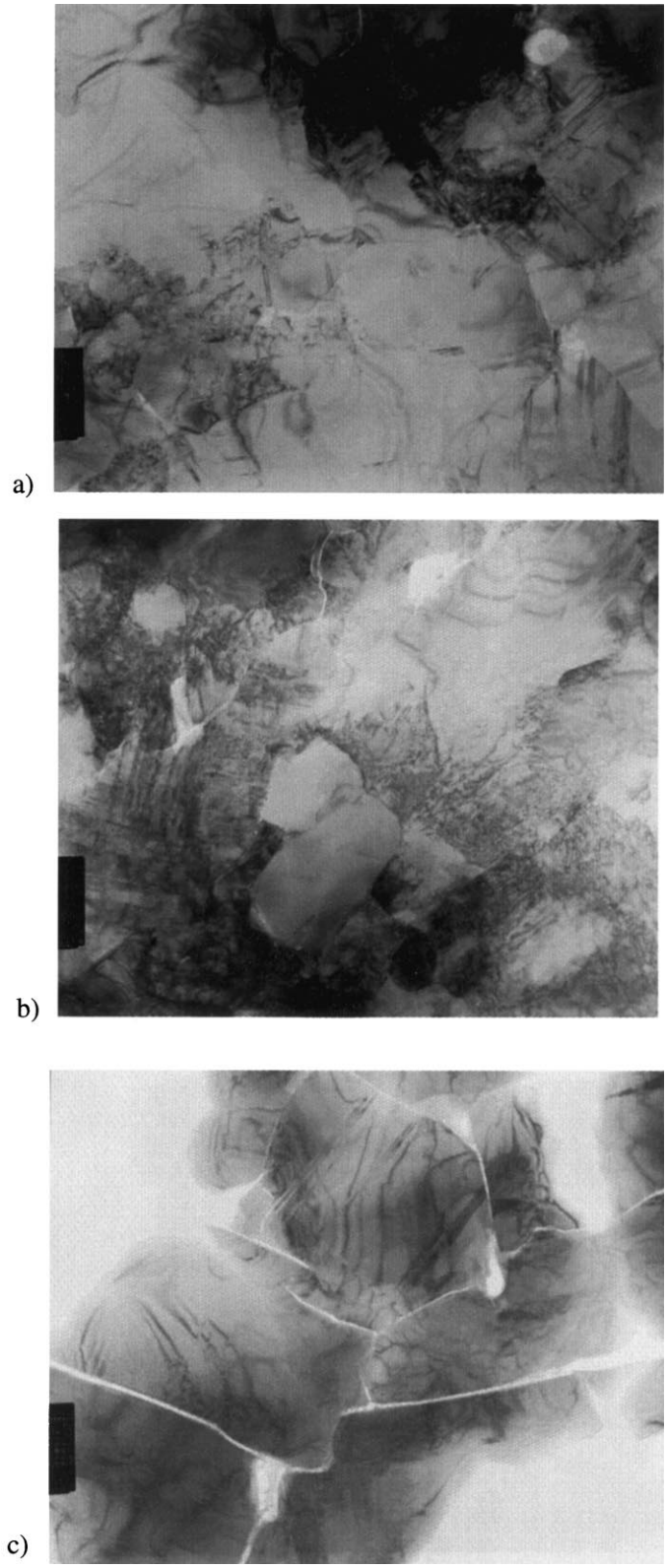

Fig. 1. TEM micrographs of three samples: (a) W816, hot-pressed starting material, long edge of micrograph is 9 μm; (b) W824, sheared by regime 1 dislocation creep, long edge of micrograph is 7 μm; (c) W539, axially compressed by solution-precipitation creep, long edge of micrograph is 9 μm.

Table 1
Experimental conditions for the measured samples; all experiments were carried out at 900°C

Sample no.	Material	Deformation geometry	'Wetness'[a,b]	Def. Mech.	Pressure (GPa)	Strain rate ($\dot{\gamma}$ or $\dot{\varepsilon}$)	Finite strain (γ or ε)	Comments
W816	Hale powder	Axial	As-is	–	1.5	Hydros.	–	Fully dense
W799	Hale powder	Simple shear	As-is	Disl. creep	1.5	6×10^{-5}/s	7.5	100% recrystallized
W824	Hale powder	Simple shear	As-is	Disl. creep	1.5	10^{-4}/s	11	100% recrystallized
RD 33	Hale core	Simple shear	0.2 wt.% water added	Disl. creep	1.5	10^{-3}/s	>50	Sample faulted at low T then deformed at high T; measurements made in shear zone
W539	Hale powder	Axial	As-is	Pres. soln.	1.0	10^{-5}/s	50%	Grain boundaries 'wetted'
W484	Hale powder	Axial	Powder v.d. at 300°C	Disl. creep	1.5	10^{-6}/s	60%	100% recrystallized
W479	Hale powder	Axial	Powder v.d. at 200°C	Disl. creep	1.5	10^{-5}/s	43%	<100% recrystallized

[a] As-is = ~0.1 wt.% adsorbed water.
[b] v.d. = vacuum dried.

intensity and unreasonably high data collection times. For the present study we therefore employed X-ray diffraction at a synchrotron source in order to investigate the CPO of fine-grained plagioclase aggregates. The high intensity of a focussed X-ray beam makes it possible to investigate fairly small volumes (here: ca. 6×10^{-4} mm^3) of polycrystalline material. The use of a two-dimensional CCD detector also provides 2Θ resolution sufficient to resolve the complicated diffraction pattern of albite and could possibly also be used for any other plagioclase composition. In the transmission geometry used here this high resolution is much less affected by defocussing effects, which create problems in the standard reflection geometry (Heidelbach et al., 1999). In comparison with measurements of single grain orientations by light-optical or SEM–EBSP methods, this technique is not limited by a small grain size and it is also relatively rapid because a large number of crystals are measured simultaneously. Compared with neutron diffraction it is not necessary to have large amounts of sample material, which is especially critical for samples experimentally deformed in simple shear, as the thickness of the shear zone is less than ~0.5 mm.

The textures were analyzed on the Microfocus beamline at the European Synchrotron Radiation Facility in Grenoble (France). Thin slabs of ca. 100-μm thickness were prepared from the experimental samples, such that they passed through the sample center and included the compression direction (and the shear direction, for sheared samples). These sections were measured in transmission geometry with a monochromatic beam ($\lambda = 0.78$ Å, Fig. 2). The X-ray beam was focussed to a diameter of 30 μm yielding a sufficient spatial resolution for the small samples. The reflections (Debye–Scherrer diffraction rings) of fourteen {*hkl*} were recorded simultaneously with a two-dimensional CCD detector. A typical spectrum derived from one measurement is shown in Fig. 3, illustrating the good resolution in 2Θ. The crystallographic planes that form a Debye–Scherrer diffraction cone lie on a small circle with an opening angle of $90-\Theta$ relative to the incoming beam. In order to fill at least a partial pole figure, the sample has to be rotated around one axis. The rotation axis was chosen parallel to the compression axis for the axial compression samples, or perpendicular to the shear plane for the simple shear samples. The rotation was carried out up to +62.5° in 5° steps, which yielded a sufficient pole figure coverage for the calculation of the orientation distribution function (ODF). The 'defocussing' of the beam due to the rotation resulted in a maximum width of the irradiated area of about 200 μm in the direction perpendicular to the rotation axis. The experimental methods are described in more detail in Heidelbach et al. (1999).

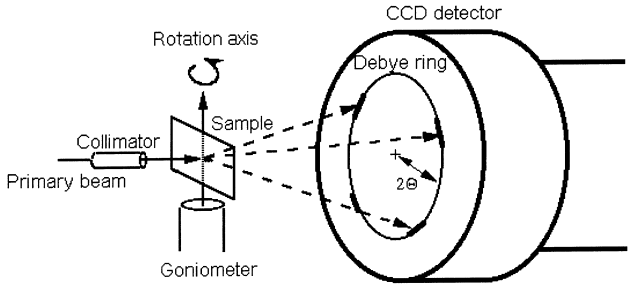

Fig. 2. Schematic sketch of the experimental setup; see text for details.

Fourteen partial pole figures were collected (Fig. 4) for each sample and used for the calculation of the complete ODF using the iterative WIMV algorithm implemented in the texture package Beartex (Wenk et al., 1998). The following crystallographic parameters for disordered (high) albite were used in the calculation (Wyckoff, 1968): $a = 8.15$ Å, $b = 12.88$ Å, $c = 7.11$Å, $\alpha = 93.4°$, $\beta = 116.3°$ and $\gamma = 90.3°$. From the ODF, complete pole figures as well as inverse pole figures could be recalculated. Comparisons between the measured and the recalculated pole figures allow us to assess the consistency of the different pole figures with each other. In Fig. 4 both sets of pole figures are shown for sample W799 as an illustration. The

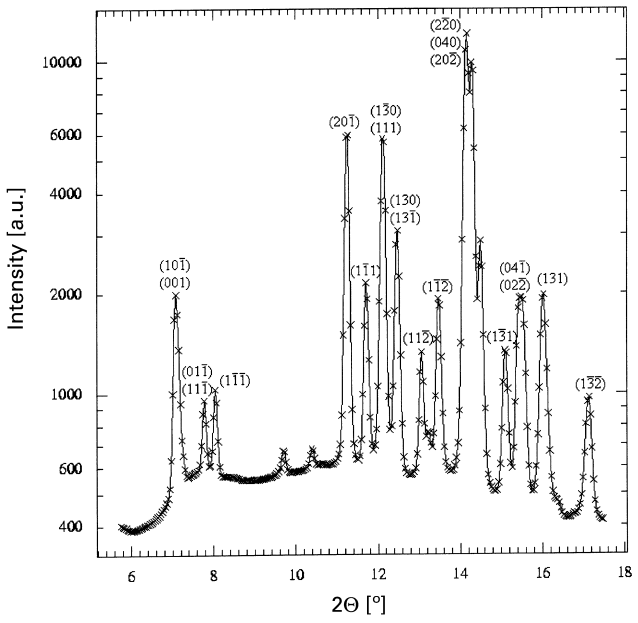

Fig. 3. Two theta profile extracted from the X-ray diffraction data ($\lambda = 0.78$ Å); the peaks that were used for the ODF calculation are indicated.

experimental pole figures contain only the data used for the ODF calculation, and not the complete Debye rings from the measurements. This limitation is due to the ODF calculation algorithm. The main features of the measured pole figures are well reproduced in the recalculated ones, although in the transitions between measured and unmeasured areas the intensity distribution is in some cases not very smooth, with 'jumps' in intensity of 0.1 to 0.2 m.r.d. (multiples of random distribution). This problem occurs for two reasons: (i) the number of pole figures used for the ODF calculation is still relatively low; and (ii) some of the peaks analyzed still contain intensity contributions from much weaker (<10%) reflections close by in 2Θ, which could not be separated in the calculation. The problem could be solved by increasing the number of measured pole figures, which would improve the coverage of the ODF space. However, the differences in the two sets of pole figures are rather minor and have very little effect on the overall CPO. We performed additional tests calculating the ODF with different sets of pole figures, leaving out those which show the discontinuities described above, and found that the overall texture pattern remained the same.

Mathematically the difference between experimental and recalculated pole figures is expressed in the so-called reproduction (RP) value which is the sum of the relative deviations between measured and recalculated pole figures (Matthies et al., 1987) in percent. For our recalculated pole figures the average RP values ranged from 3 to 10% (Table 2), which we consider satisfactory. In order to test the influence of single pole figures on the resulting CPO we performed a number of ODF calculations using different sets of pole figures for the same sample. In all cases the resulting ODFs were very similar to the ODF calculated from all pole figures for one sample. The recalculated pole figures illustrated in Figs. 5–8 were derived from ODFs which were smoothed with a Gaussian function of 7.5° full width half maximum.

Due to the triclinic symmetry of albite ($\bar{1}$) upper and lower hemisphere projections are distinguished and have different intensity distributions. This symmetry is preserved in the calculations described above and reflected in the orientation distributions illustrated in Figs. 5–8. However, on a statistical basis the CPOs display at least monoclinic symmetry, imposed by the deformation geometry, which is monoclinic in the case of simple shear experiments and axially symmetric in the case of axial compression. Therefore we were able to project all of the orientation data for one pole figure into one (the lower) hemisphere without any loss of information.

3. Results

3.1. Microstructures

The experimental samples have a very fine grain size, which makes it almost impossible to study the microstructure in the light microscope. Therefore TEM observations were used to infer the dominant deformation mechanisms. Most samples consist of very small (<2 μm) polygonal grains with tight grain boundaries. The dislocation density is quite variable from grain to grain and also within single grains (Fig. 1b); in many places one can observe a dislocation-free grain bulging into and apparently replacing a neighbor grain with a high dislocation density. Most dislocations are tangled; no low angle boundaries were observed. The absence of subgrains and the variability in dislocation density indicate deformation by low-temperature recrystallization-accommodated dislocation creep (e.g., regime 1 of Hirth and Tullis, 1992).

One sample, deformed with ~0.1 wt.% adsorbed water, has a slightly larger grain size (5–10 μm) and a very different microstructure (W539; Fig. 1c). TEM shows that most grains are euhedral and lath-shaped. All grains have very low dislocation density, and all orientations of grain boundaries appear to be open and 'wetted' (see Tullis et al., 1996, for details). This microstructure indicates deformation by solution-precipitation creep, rather than dislocation creep.

3.2. Textures

The CPOs in all the samples described below are relatively weak, with maximum intensities of 2.5 to 3 m.r.d. The hot-pressed sample as well as all three samples deformed in axial compression show CPOs with orthorhombic rather than axisymmetric symmetry, due to the sectioning of the sample and the fact that only a single planar 'slice' was measured. The complete axisymmetric texture would only

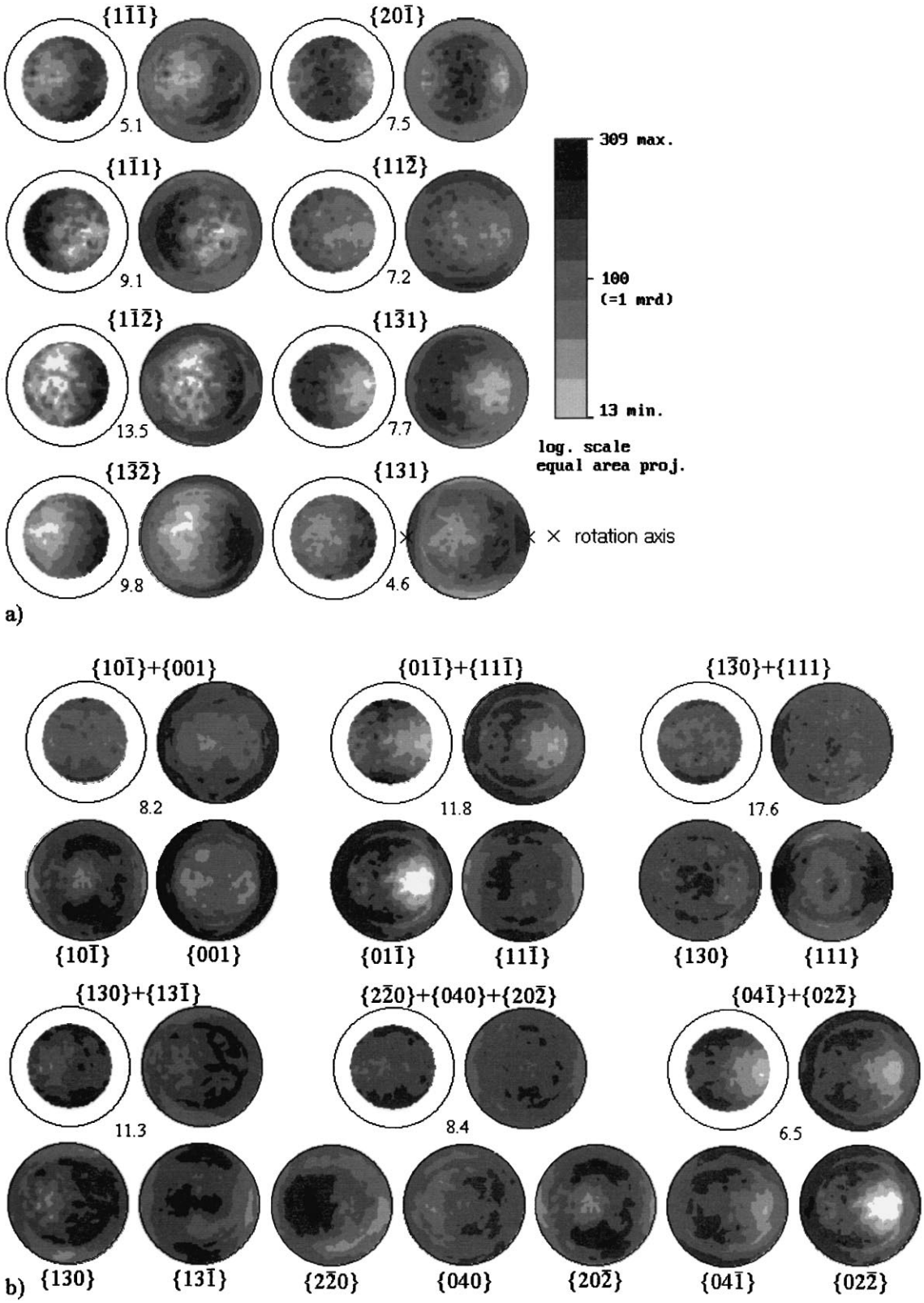

Fig. 4. Comparison of incomplete measured and complete recalculated pole figures for sample W799. (a) Pole figures of single {*hkl*}; small numbers indicate the RP value for each pole figure; the projection is onto the sectioning plane and the position of the rotation axis of experimental setup (see Fig. 2) is marked. (b) Pole figures of overlapped {*hkl*}, with RP values indicated. The combined as well as the separated pole figures derived from the recalculated data set are shown; intensity scale is the same as in (a).

Table 2
Data from calculation of ODF

Sample	RP[a]	RP1[b]	No. of iteration steps
W816	7.07	5.83	14
W536	10.03	7.66	17
W479	10.37	7.25	14
W479 (lens)	9.85	7.89	11
W479 (flat lens)	3.12	2.81	7
W484	4.72	3.78	11
W799	8.36	6.61	13
W824	9.45	6.90	13
RD33	10.47	8.93	15

[a] Reproduction value averaged over all pole figures.
[b] Reproduction value for all data points > 1 m.r.d. averaged over all pole figures.

be revealed if the entire sample cylinder was measured; a single radial section through this cylinder only contains part of the axisymmetric CPO. Artificially imposing axial symmetry about the compression axis into the experimental data set generally worsened the results of the ODF calculation (e.g. RP values) and was therefore not pursued.

3.2.1. Hot-pressed sample

The hot-pressed starting material (W816, Fig. 5) shows a weak preferred orientation; the poles to the {100} and {001} planes as well as the <100> directions have higher concentrations perpendicular to the sample cylinder axis. Albite has two perfect cleavages, {001} and {010}, so this texture may have been produced by top loading of the 2–10-μm albite grains into the Pt can, resulting in cleavage-bounded laths lying perpendicular to the cylinder axis.

3.2.2. Axial compression

All three samples deformed in axial compression (W539, W484, W479; Figs. 6 and 7) show a CPO that is distinctly different from that of the hot-pressed sample. In all the deformed samples the poles to the {001} planes form broad maxima subparallel to the compression direction.

The CPO for the sample deformed by solution-precipitation

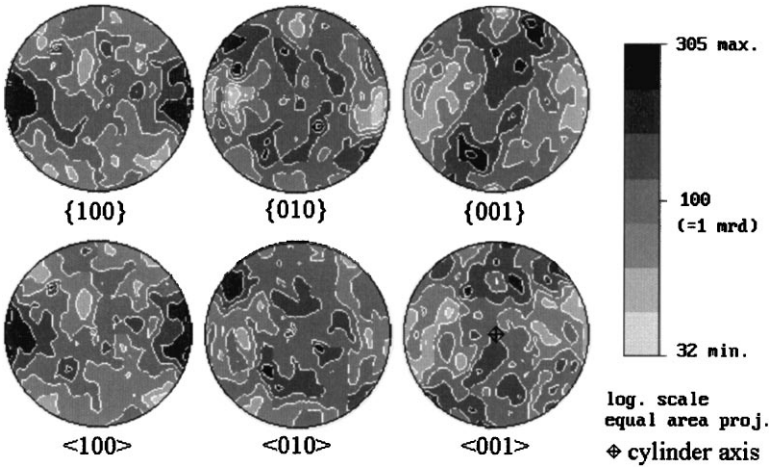

Fig. 5. Pole figures for hot pressed starting material (W816); trace of the sectioning plane of the sample lies horizontal (E–W).

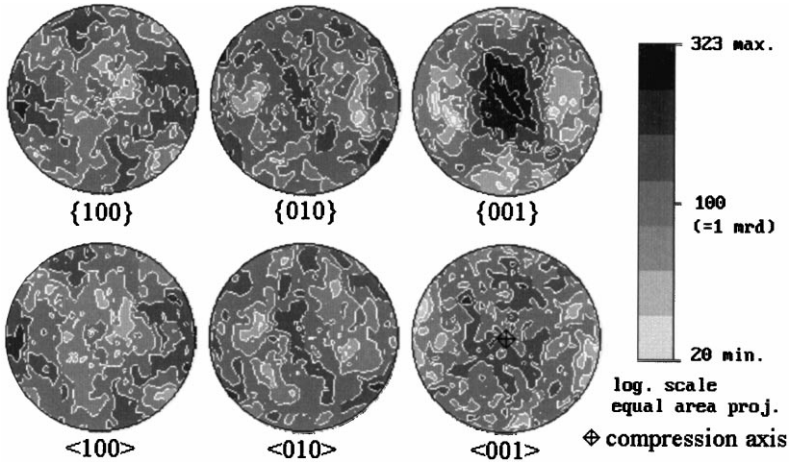

Fig. 6. Pole figures for sample deformed in axial compression by solution-precipitation creep (W539); trace of the sectioning plane of the sample lies horizontal (E–W).

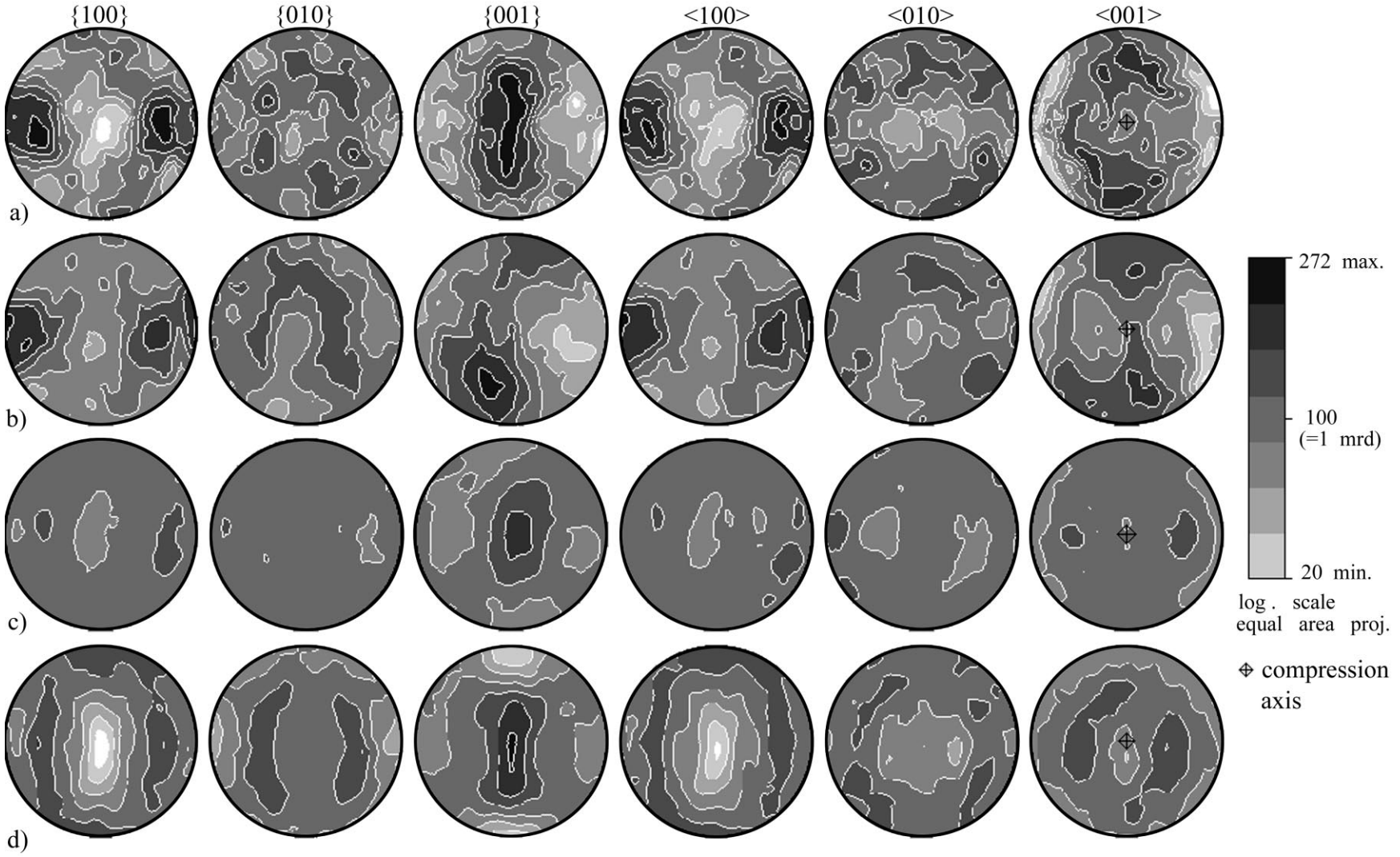

Fig. 7. Pole figures for samples deformed in axial compression by dislocation creep: (a) W479, 43% strain; (b) coarse-grained lens in sample W479; (c) extremely flattened and fine-grained lens in sample W479; (d) W484, 60% strain; trace of the sectioning plane of the sample lies horizontal (E–W).

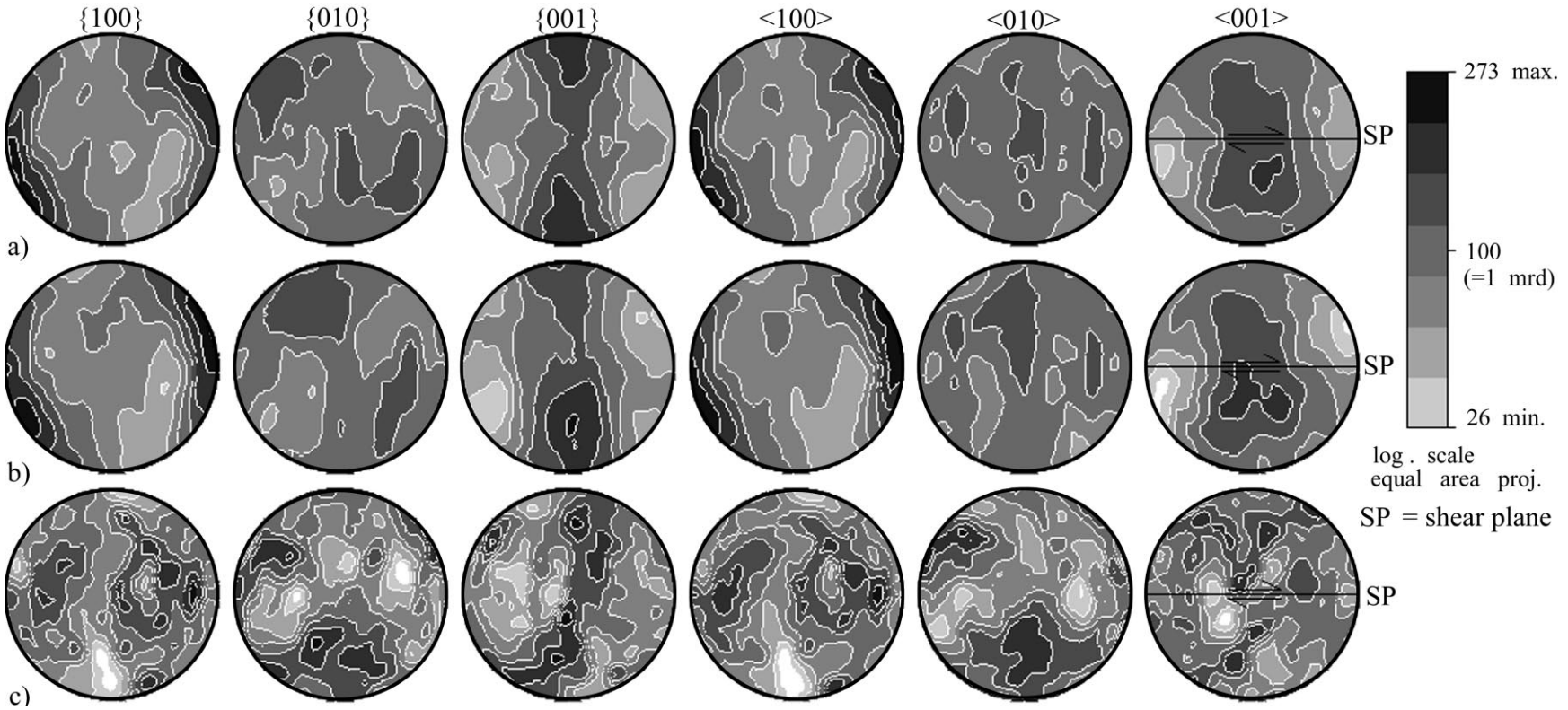

Fig. 8. Pole figures of samples deformed in simple shear: (a) W799, $\gamma \sim 7.5$; (b) W824, $\gamma \sim 11$; (c) RD33, $\gamma > 50$.

creep (W539) is shown in Fig. 6. The poles to {100} as well as the <100> and <010> directions are predominantly perpendicular to the compression direction, while the poles to {001} as well as the <001> directions are aligned parallel to the compression direction.

The CPOs for the two samples deformed by dislocation creep are shown in Fig. 7. In addition to the bulk textures for samples W479 (Fig. 7a, 43% strain) and W484 (Fig. 7d, 60% strain), we also show measurements from two small lens-shaped regions inside sample W479; one was a more coarse-grained lens which was not highly flattened (Fig. 7b), and the second (Fig. 7c) was an extremely flattened and fine-grained lens. Both probably originated as thin 'crusts' produced by drying of the size-settled powder, which were insufficiently homogenized with the bulk material. These lenses were located close to the center of the sample, where the bulk measurement was carried out.

All four textures in Fig. 7 are characterized by strong maxima of the poles to {001} subparallel to the compression axis. The bulk CPO for samples W484 and W479 also show maxima of the poles to {100} and the <100> and <010> directions close to 90° from the compression axis. The poles to {010} form an almost-complete small circle around the compression axis. The coarse-grained lens in sample W479 displays a very similar pattern, which is however rotated about 45° around a horizontal axis (lying about E–W in the plane of the figure). In contrast, the fine-grained lens shows very little preferred orientation, with only a weak maximum of the poles to {001} parallel to the compression axis.

3.2.3. Simple shear deformation

The three samples deformed in simple shear by dislocation creep also display CPOs of {001} (Fig. 8). In two samples (W799, W824) with shear strains of 7.5 and 11, respectively, this plane is aligned subparallel to the shear plane. The poles to {100} and the <100> directions form broad maxima that extend from the shear direction to about 30° rotated against the sense of shear, whereas the {010} planes show little preferential alignment.

In the third sample (RD33), with a very high shear strain (>50), the poles to {001} form a girdle which is oblique to the shear plane and slightly rotated with the shear sense. The macroscopic position of the shear plane in this sample is not as clearly defined as that in the other two samples, because it was produced by faulting rather than by making a saw-cut. Neither the {100} nor the {010} planes display a strong CPO in this sample. Generally the distribution appears to be much more 'noisy' and less smooth. For samples W799 and W824 the monoclinic symmetry of the deformation is nicely reflected in the CPO pattern. For RD33, where the strain geometry was less-clearly defined, the texture deviates more strongly from monoclinic symmetry.

4. Discussion

4.1. Introduction

Several slip systems have been identified with TEM in experimentally and naturally deformed plagioclases (e.g. Olsen and Kohlstedt, 1984; Marshall and McLaren 1977a,b; Montardi and Mainprice, 1987), but relatively little is known from experiments or nature about the relative activity of different slip systems in plagioclase under varying deformation conditions. In addition, there are relatively few published CPOs for plagioclase, and they have been derived from a wide range of metamorphic and deformation conditions, chemical composition of the plagioclase phase, and overall rock compositions. At present no consistent empirical hypothesis for the interpretation of plagioclase CPOs has been proposed, and to our knowledge there have been no attempts to model the CPO development in plagioclase numerically. We will therefore begin our interpretation of the pole figures for the dislocation creep samples based on the alignment of known or inferred slip systems with the deformation geometry. We will then discuss the effects of dynamic recrystallization and the possible causes for the CPO developed in the solution-precipitation creep sample, and will conclude by comparing the experimental textures with those measured optically for naturally deformed plagioclase.

4.2. CPO produced by dislocation creep

First it should be noted that the axially deformed samples have their {001} planes strongly rotated with respect to those in the hot-pressed starting material. Thus the textures measured in the deformed samples are not just inherited from the hot-pressing stage of the experiments.

The preferential alignment of the {001} planes in samples deformed by dislocation creep, either perpendicular to the compression direction or parallel to the shear plane, indicates that this plane has served as the principal glide plane during dislocation creep. During axial compression, the dominant slip planes tend to rotate towards a position perpendicular to the axis of compression. As they do so, the resolved shear stress on those planes decreases. During simple shear, the dominant slip planes rotate least rapidly in orientations close to the shear plane, and the slip direction tends to align parallel to the shear direction (e.g. Wenk and Christie, 1991). The alignment of <100> in the shear direction in W799 and W824 suggests that {001}<100> slip may have been the dominant slip system in the samples deformed by simple shear.

The textures in the two lens-shaped regions in sample W479 are rather interesting. The weak CPO in the extremely flattened and very fine-grained lens may result from an increased component of diffusion creep and grain boundary sliding in this region compared with the coarser-grained matrix. The coarse-grained lens, on the other hand, was

apparently stronger and thus less deformed than the matrix. The origin of the asymmetry in its CPO relative to the compression axis is not clear.

The effect of dynamic recrystallization on CPO development, especially in the low-temperature dislocation creep regime, is not yet well understood. In metals it is known that the rate of grain boundary migration is a function of the orientation of the grain boundary with respect to the crystal lattices (e.g Gottstein and Shvindlerman, 1999), but how this affects the overall CPO in bulk samples is not understood. Gleason et al. (1993) studied axially shortened novaculites deformed in the same low-temperature dislocation creep regime as our albite samples; they found that during bulging recrystallization dislocation-free 'hard'-grains grew at the expense of 'soft' grains with a higher dislocation density. The bulk CPO shows a broad maximum of poles to the easy {001} slip plane parallel to the compression direction. In plagioclase, {001} is inferred to be an easy slip plane (e.g. Kruse, 1998, Kruse and Stünitz, 1999), and we observe that poles to {001} form a maximum parallel to the compression direction. This similarity suggests that the same process may operate during low-temperature bulging recrystallization in quartz and albite.

The relatively low strengths of the CPOs in all our samples seem puzzling. Our study was motivated, in part, by the very strong extinction and gypsum plate effects that we had observed in the samples optically. Thus one result is that optical flat stage effects are not as accurate an indication of CPO strength for this biaxial mineral as they are for quartz. The relatively low strengths of the CPOs are also puzzling considering the high strains (γ of 7.5 to 50) in the sheared samples. The weakness of the pattern may reflect in part the influence of dynamic recrystallization, but at present we cannot evaluate this possibility because we do not have CPOs from samples of distinctly different degrees of recrystallization. The weakness may also reflect a component of grain boundary sliding in these very fine-grained aggregates. Unfortunately grain boundary sliding leaves no microstructural evidence, optically or in TEM, and there are as yet no flow-law data to provide independent evidence for a contribution from this process.

4.3. CPO produced by solution precipitation creep

The slightly different CPO found for sample W539 suggests that solution-precipitation creep produces a CPO distinct from that produced by dislocation creep. The distinction is subtle: all samples deformed in axial compression have a maximum of poles to {001} parallel to the compression direction, but only in sample W539 do the poles to {010} tend to lie perpendicular to the compression direction.

Solution-precipitation creep involves dissolution on grain faces under higher normal stress and precipitation on grain faces under lower normal stress, driven by the difference in chemical potential between these sites; the rate-limiting process may be either dissolution/reprecipitation or grain boundary diffusion. There are several possible factors which may allow this deformation mechanism to produce a CPO (Bons and Den Brok, 1999): (i) chemical potential anisotropy, (ii) preferential precipitation sites (cracks, cleavage), and (iii) anisotropy of dissolution and/or growth rates. Although there are no data with which to make a specific calculation, the albite crystal structure is highly anisotropic, and thus it is quite likely that anisotropy of chemical potential or of dissolution and growth rates may have been responsible for the CPO. The observed {001} maximum might result from slow growth parallel to $<001>$ or perhaps to preferential precipitation on the {010} cleavage plane.

Anisotropy of dissolution or growth can only be important in producing a CPO if diffusion is fast with respect to the interface reactions (Bons and Den Brok, 1999). Recent measurements show that grain boundary diffusion in feldspars is quite fast (Yund and Farver, 1999). A strong indication that grain boundary diffusion in our sample W539 was relatively fast is provided by TEM observations showing open grain boundaries that apparently were 'wetted' during the deformation, suggesting that diffusivities may have approached those for a bulk fluid (Tullis et al., 1996).

4.4. Comparison with natural plagioclase CPOs

The CPOs in our sheared samples deformed by dislocation creep suggest that $\{001\} < 100 >$ may have been the dominant slip system. Similar CPOs have been measured by several authors for plagioclase in high-grade rocks. Kruhl (1987a) and Siegesmund et al. (1994) observed that for plagioclase in amphibolite facies rocks, the {001} planes were subparallel to the macroscopic foliation and the $<100>$ directions were subparallel to the lineation. A similar alignment of the {001} planes with the foliation and $<100>$ directions with the lineation was found in plagioclase from a mylonitic granulite by Ullemeyer and Weber (1999). However, detailed comparisons with our experimental samples are not warranted because in all these studies the plagioclase was more anorthitic and it was not the only phase in the rock. In addition, the alignment of $\{001\} < 100 >$ that developed in our experimental samples resulted from low-temperature (regime 1) dislocation creep, equivalent to upper greenschist to middle amphibolite facies conditions for naturally deformed rocks (Post and Tullis, 1999), whereas the similar CPOs reported in the studies cited above were for amphibolite to granulite facies. From his observations of naturally deformed plagioclase Kruhl (1987a,b) suggests that the $\{001\} < 100 >$ slip system may be more active in rocks of higher grade and/or with higher An content, but these inferences are not consistent with our experimental results.

The $\{010\} <001>$ slip system is also inferred to be common in naturally deformed plagioclase (e.g. Olsen and

Kohlstedt, 1984, 1985; Ji et al. 1988; Ji and Mainprice, 1990; Kruhl 1987a,b; Kruse and Stünitz, 1999). From the CPO patterns we measured, it does not appear that this system played an important role during the plastic deformation of our samples. The microstructures described by Ji et al. (1988) suggest that their samples deformed by regime 2 (rotation recrystallization) dislocation creep, and thus at relatively higher temperature conditions than in our experiments. The difference in dominant slip system may be due to those different conditions. However, the positions of maxima in the {010} and <001> pole figures for some of our samples (W479, W484) are consistent with a component of dislocation glide on this slip system.

Several studies have reported that both slip systems {001}<100> and {010}<001> were active simultaneously. Kruhl (1987a,b) inferred from CPO patterns that both slip systems were active in plagioclase from amphibolite and greenschist facies rocks near the Insubric line (western Alps). FitzGerald et al. (1983) used TEM to study albite naturally deformed under blueschist grade conditions, and found that slip on {010} and {001} planes dominated. Their microstructures suggest that deformation occurred by a combination of regime 1 and 2 dislocation creep.

Several slip systems have been determined from previous studies of experimentally deformed plagioclase. Marshall and McLaren (1977a,b) determined the dominant slip system in single crystals of albite oriented with the compression direction bisecting the acute angle between {010} and {001} and deformed at 800°C, 1000 MPa and 10^{-5}/s, i.e., regime 1 dislocation creep conditions. Although microfracturing was the dominant deformation mechanism, they found evidence for slip on $\{10\bar{1}\}$, different from the dominant slip on {001} that we infer in the recrystallized albite aggregates.

The CPOs of the experimentally sheared samples (especially W799, W824) show a marked asymmetry of the <100> maxima with respect to the shear zone boundaries that could be used for the determination of the shear sense if this type of texture was found in a naturally deformed sample. The published CPOs showing {001}<100> textures (see above) do not show any asymmetry except one sample (#705) of Kruhl (1987a). In that case it is the {001} maximum that shows a marked asymmetry relative to the macroscopic fabric coordinates.

Further comparisons of our experimental CPOs with those from naturally deformed plagioclase remain problematic due to the chemical heterogeneity of this material and the possible influence of other phases in natural samples. In addition, there are no predictions from polycrystal plasticity simulations to use as a reference.

5. Conclusions

The present study is the first to measure CPOs from experimentally deformed albite aggregates. The patterns indicate that dislocation glide on the {001}<100> slip system is active in the samples deformed by recrystallization-accommodated (regime 1) dislocation creep at the given experimental conditions, although we cannot evaluate the effects of dynamic recrystallization or a possible contribution from grain boundary sliding. Solution precipitation creep appears to produce a distinct CPO. In the samples deformed in simple shear the monoclinic symmetry of the deformation is reflected in the CPOs and may possibly be used as a tool to determine the shear geometry in natural samples. With newly developed methods such as the one described here or electron backscattering (Prior and Wheeler, 1999) it should be possible to broaden the basis for the interpretation of textures in feldspars.

Acknowledgements

H. Stünitz and M. Casey are thanked for their thorough reviews which greatly improved the original manuscript.

References

Bons, P.D., Den Brok, B.W.J. 2000. Crystallographic preferred orientation development by dissolution precipitation creep. Journal of Structural Geology, submitted.

Burri, C., Parker, R.L., Wenk, E., 1967. Die optische Orientierung der Plagioklase. Birkhäuser, Basel.

Dell'Angelo, L.N., Tullis, J., 1989. Fabric development in experimentally sheared quartzites. Tectonophysics 169, 1–21.

FitzGerald, J.D., Etheridge, M.A., Vernon, R.H., 1983. Dynamic recrystallization in a naturally deformed albite. Textures and Microstructures 5, 219–237.

Gleason, G.C., Tullis, J., Heidelbach, F., 1993. The role of dynamic recrystallization in the development of lattice preferred orientations in experimentally deformed quartz aggregates. Journal of Structural Geology 15, 1145–1168.

Gottstein, G., Shvindlerman, L.S., 1999. Grain boundary migration in metals: Thermodynamics, kinetics, applications. CRC Press, Boca Raton, FL.

Heidelbach, F., Riekel, C., Wenk, H.R., 1999. Quantitative texture analysis of small domains with synchrotron X-rays. Journal of Applied Crystallography 32, 841–849.

Hirth, G., Tullis, J., 1992. Dislocation creep regimes in quartz aggregates. Journal of Structural Geology 14, 145–159.

Ji, S., Mainprice, D., Boudier, F., 1988. Sense of shear in high temperature movement zones from the fabric asymmetry of plagioclase feldspars. Journal of Structural Geology 10, 73–81.

Ji, S., Mainprice, D., 1990. Recrystallization and fabric development in plagioclase. Journal of Geology 98, 65–79.

Ji, S., Zhao, X., Zhao, P., 1994. On the measurement of plagioclase lattice preferred orientation. Journal of Structural Geology 16, 1711–1718.

Kruhl, J.H., 1987a. Preferred lattice orientations of plagioclase from amphibolite and greenschist facies rocks near the Insubric Line (Western Alps). Tectonophysics 135, 233–242.

Kruhl, J.H., 1987b. Zur Deformation und Gitterregelung des Plagioklases. Jahrbuch der Geologie—Bundesanstalt Wien 130, 205–243.

Kruse, R. 1998. Recrystallization and deformation mechanisms in mafic high temperature mylonites from the Jotun nappe (S. Norway) and the Ivrea zone (N. Italy). Ph.D. thesis, Universität Basel.

Kruse, R., Stünitz, H., 1999. Deformation mechanisms and phase distribution in mafic high-temperature mylonites from the Jotun Nappe, southern Norway. Tectonophysics 303, 223–249.

Lister, G.S., Hobbs, B.E., 1980. The simulation of fabric development during plastic deformation and its application to quartzite: the influence of deformation history. Journal of Structural Geology 2, 355–370.

Mainprice, D., Bouchez, J.-L., Blumenfeld, P., Tubia, J.M., 1986. Dominant c slip in naturally deformed quartz: Implications for dramatic plastic softening at high temperature. Geology 14, 819–822.

Marshall, D.B., McLaren, A.C., 1977a. Deformation mechanisms in experimentally deformed plagioclase feldspars. Physics and Chemistry of Minerals 1, 351–370.

Marshall, D.B., McLaren, A.C., 1977b. The direct observation and analysis of dislocations in experimentally deformed plagioclase feldspars. Journal of Materials Science 12, 893–903.

Matthies, S., Vinel, G.W., Helming, K., 1987. Standard Distributions in Texture Analysis. Akademie Verlag, Berlin.

Montardi, Y., Mainprice, D., 1987. A transmission electron microscopic study of the natural plastic deformation of calcic plagioclases (An 68–70). Bulletin de Mineralogie 110, 1–14.

Olsen, T.S., Kohlstedt, D.L., 1984. Analysis of dislocations in some naturally deformed plagioclase feldspars. Physics and Chemistry of Minerals 11, 153–160.

Olsen, T.S., Kohlstedt, D., 1985. Natural deformation and recrystallization of some intermediate plagioclase feldspars. Tectonophysics 111, 107–131.

Post, A., Tullis, J., 1999. A recrystallized grain size piezometer for experimentally deformed feldspar aggregates. Tectonophysics 303, 159–173.

Prior, D.J., Wheeler, J., 1999. Feldspar fabrics in a greenschist facies albite-rich mylonite from electron backscatter diffraction. Tectonophysics 303, 29–49.

Schmid, S.M., 1994. Textures of geological materials: computer model predictions versus empirical interpretations based on rock deformation experiments and field studies. In: Bunge, H.-J., Siegesmund, S., Skrotzki, W., Weber, K. (Eds.), Textures of Geological Materials, Deutsche Gesellschaft für Metallkunde, Oberursel, pp. 279–301.

Schmid, S.M., Panozzo, R., Bauer, S., 1987. Simple shear experiments on calcite rocks: rheology and microfabric. Journal of Structural Geology 9, 747–778.

Siegesmund, S., Helming, K., Kruse, R., 1994. Complete texture analysis of a deformed amphibolite: comparison between neutron diffraction and U-stage data. Journal of Structural Geology 16, 131–142.

Tullis, J., 1990. Experimental studies of deformation mechanisms and microstructure in quartzo-feldspathic rocks. In: Barber, D.J., Meredith, P.G. (Eds.), Deformation Processes in Minerals, Ceramics and Rocks, Mineralogical Society series 1, pp. 190–227.

Tullis, J., Christie, J.M., Griggs, D.T., 1973. Microstructures and preferred orientations of experimentally deformed quartzites. Geological Society of America Bulletin 84, 297–314.

Tullis, J., Dell'Angelo, L.N., Yund, R.A., 1990. Ductile shear zones from brittle precursors in feldspathic rocks: the role of dynamic recrystallization. In: Duba, A.G., Durham, W.B., Handin, J.W., Wang, H.F. (Eds.), American Geophysical Union Monograph 56, pp. 67–81.

Tullis, J, Yund, R., Farver, J., 1996. Deformation-enhanced fluid distribution in feldspar aggregates and implications for ductile shear zones. Geology 24, 63–66.

Ullemeyer, K., Helming, K., Siegesmund, S., 1994. Quantitative texture analysis of plagioclase. In: Bunge, H.-J., Siegesmund, S., Skrotzki, W., Weber, K. (Eds.), Textures of Geological Materials, Deutsche Gesellschaft für Metallkunde, Oberursel, pp. 93–108.

Ullemeyer, K., Weber, K., 1999. Lattice preferred orientation as an indicator of a complex deformation history of rocks. Textures and Microstructures 33, 45–60.

Wenk, H.-R., Bunge, H.J., Jansen, E., Pannetier, J., 1986. Preferred orientation of plagioclase-neutron diffraction and U-stage data. Tectonophysics 126, 271–284.

Wenk, H.-R., Matthies, S., Donovan, J., Chateigner, D., 1998. BEARTEX: a Windows-based program system for quantitative texture analysis. Journal of Applied Crystallography 31, 262–269.

Wenk, H.-R., Christie, J.M., 1991. Review paper: comments on the interpretation of deformation textures in rocks. Journal of Structural Geology 13 (10), 1091–1110.

Wenk, H.-R., Pannetier, J., 1990. Texture development in deformed granodiorites from the Santa Rosa mylonite zone, southern California. Journal of Structural Geology 12, 177–184.

Wyckoff, R.W.G., 1968. Crystal Structures. Interscience Publishers, New York.

Yund, R., Farver, J., 1999. Si grain boundary diffusion rates in feldspar aggregates, EOS, Transactions American Geophysical Union, 80, 974.